Thickness-dependent insulator-to-metal transition in epitaxial RuO$_2$ films

Anil Kumar Rajapitamahuni,[1,*] Sreejith Nair [ORCID],[1] Zhifei Yang,[1,2] Anusha Kamath Manjeshwar [ORCID],[1]
Seung Gyo Jeong,[1] William Nunn,[1] and Bharat Jalan[1,†]

[1]*Department of Chemical Engineering and Materials Science, University of Minnesota, Minneapolis, Minnesota 55455, USA*
[2]*School of Physics and Astronomy, University of Minnesota, Minneapolis, Minnesota 55455, USA*

Epitaxially grown RuO$_2$ films on TiO$_2$ (110) exhibit significant in-plane strain anisotropy, with a compressive strain of -4.7% along the [001] crystalline direction and a tensile strain of $+2.3\%$ along [1$\bar{1}$0]. As the film thickness increases, anisotropic strain relaxation is expected. By fabricating Hall bar devices with current channels along two in-plane directions, $\langle 001 \rangle$ and $\langle 1\bar{1}0 \rangle$, we reveal anisotropic in-plane transport in RuO$_2$/TiO$_2$ (110) films grown via the solid-source metal-organic molecular beam epitaxy approach. For film thicknesses (t_{film}) $\leqslant 3.6$ nm, the resistivity along $\langle 001 \rangle$ exceeds that along the $\langle 1\bar{1}0 \rangle$ direction at all temperatures. With further decrease in film thickness, we uncover a transition from metallic to insulating behavior at $t_{film} \leqslant 2.1$ nm. Our combined temperature- and magnetic field-dependent electrical transport measurements reveal that this transition from metallic to insulating behavior is driven by electron-electron interactions.

I. INTRODUCTION

Rutile ruthenium dioxide (RuO$_2$) holds significant technological importance due to its exceptional properties. It possesses high electrical conductivity and exhibits excellent thermal and chemical stability. These attributes render RuO$_2$ invaluable in applications such as catalysis, serving as an electrode material in energy storage devices, and acting as diffusion barriers in microelectronic devices [1]. From the perspective of correlated physics and magnetism, RuO$_2$ stands out as a 4d transition metal oxide (TMO) characterized by comparable bandwidths and on-site Coulomb repulsion energies. This unique combination of properties makes it intriguing, yet its behavior is not fully understood [2].

RuO$_2$ was long believed to be a Pauli paramagnet [3]. However, recent findings from polarized neutron diffraction [4] and resonant x-ray diffraction [5] studies challenge this notion. They provide evidence of an itinerant antiferromagnetic (AFM) ground state with a Néel temperature exceeding 300 K, and the Néel vector predominantly aligned along the c axis. The AFM metallic properties of RuO$_2$, which is now established as an altermagnetic material [6–8], open up exciting possibilities for novel spintronics applications, including spin splitting torque [9–11] and AFM tunnel junction devices [12].

Similarly, the carrier transport properties of RuO$_2$ were thought to exhibit normal metallic behavior governed by electron-phonon and electron-electron interactions [13–16]. However, recent studies suggest RuO$_2$ is a Dirac nodal line semimetal with flat band surface states [17] and is theoretically proposed to host a novel crystal Hall effect [18], thereby reviving itself as a quantum material. Furthermore, super-

conductivity has been observed below 2 K in thin films of RuO$_2$ grown on TiO$_2$ (110) substrates and the T_c depends on the film thickness [19,20]. No superconductivity is observed when thin films were grown on MgF$_2$ (110) substrates with similar crystal orientation but with smaller lattice mismatch. These findings suggest that strain might play an important role in the electronic properties of RuO$_2$ films. Additionally, it is noteworthy that RuO$_2$/TiO$_2$ (110) displays pronounced in-plane strain anisotropy with a compressive strain of -4.7% along the [001] crystalline direction and a tensile strain of $+2.3\%$ along the [1$\bar{1}$0] direction. This anisotropic strain is known to sensitively affect the electronic structure leading to an enhanced Fermi level density of states from orbitals in the plane of the RuO$_2$ (110) film [19,21] along with an upshift of the unoccupied e_g orbitals to higher energies [22]. Hence, the ground state electronic properties are further expected to exhibit a high sensitivity to variations in film thickness as the epitaxial strain relaxes.

In this work, we systematically vary the thickness (t_{film}) of RuO$_2$ films grown directly on TiO$_2$ (110) substrates to investigate their temperature-dependent magnetotransport properties, and anisotropic transport behavior along two in-plane crystallographic directions, [001] and [1$\bar{1}$0]. With decreasing t_{film}, we observe a transition from metallic to insulatinglike electrical transport behavior. The temperature-dependent carrier transport properties at large thicknesses are primarily governed by electron-phonon interactions. The transition from metallic to insulating state in ultrathin films coincides with upturn in resistivity at low temperatures which can be explained by localization effects. Magnetotransport studies reveal electron-electron interactions (EEI) play an important role at low temperatures at these thicknesses and can be explained by the theory of weak antilocalization. Insulating behavior was observed for $t_{film} < 2$ nm and is explained by strong localization which is likely due

*Contact author: arajapita1@bnl.gov
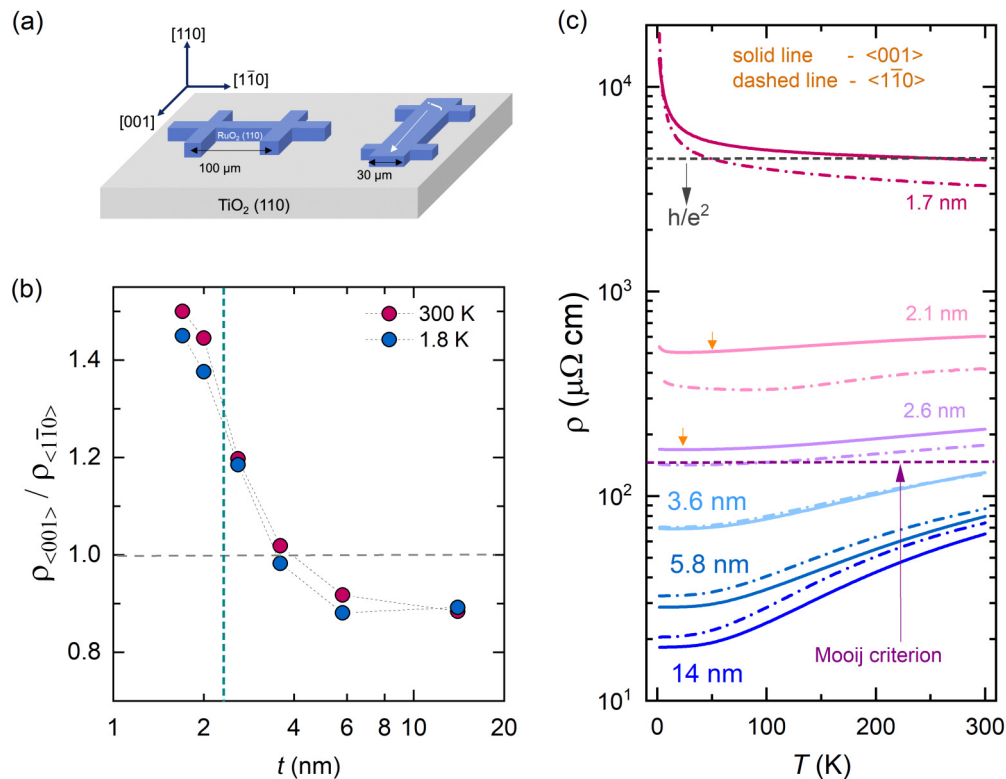†Contact author: bjalan@umn.edu

FIG. 1. (a) Schematic of thin film Hall bar devices with current channels along the in-plane crystalline directions. (b) Ratio of resistivity along two orthogonal in-plane directions as a function of thickness (t) at 300 and 1.8 K. The vertical dashed line separates the metallic and insulating regimes. (c) Resistivity vs temperature for different film thicknesses. The two orange arrows mark the temperature at which upturn in the resistivity occurs.

to disorder or other unknown effects at the substrate/film interface.

II. EXPERIMENT

Epitaxial RuO_2 films with smooth surfaces on TiO_2 (110) substrates were grown using a solid-source metal-organic molecular beam epitaxy (MBE) technique [23,24]. Details of growth conditions and structural characterization for different film thicknesses can be found in Ref. [25] and Fig. S1 of the Supplemental Material [26]. Briefly, we summarize them here. All RuO_2/TiO_2 (110) films were single crystalline with smooth surfaces. Films remained continuous even in the ultrathin limit as shown in the atomic force microscope image in Fig. S1(b) [26] with a root mean square roughness of $1-2$ Å. The analysis of reciprocal space maps suggests the films are epitaxial with an onset of strain relaxation occurring at a thickness as small as 6 nm [25].

The (110)-oriented TiO_2 substrates provide anisotropic strain to the RuO_2 film, resulting in a larger out of plane lattice parameter in thin films of RuO_2 compared to the bulk value (3.176 Å) [25]. To understand the effect of anisotropic strain on the transport properties, Hall bars with current channels along the $\langle 001 \rangle$ and $\langle 1\bar{1}0 \rangle$ crystallographic directions were fabricated as shown in Fig. 1(a). The fabrication of Hall bars is carried out using photolithography followed by argon ion milling. Electrical contacts are made by

Aluminum wire bonding. The channel resistance was measured with direct current (dc) of 100 nA–10 µA, using a Keithley 2430 source-measure unit. Temperature-dependent transport measurements were performed between 1.8 and 300 K in a Quantum Design Dynacool Physical Property Measurement System (PPMS) equipped with a superconducting 9 T magnet.

III. RESULTS AND DISCUSSION

We examine the influence of film thickness on the electrical resistivity (ρ) in relation to temperature (T) using the Hall bar devices along both crystalline directions as shown in Fig. 1(b). As t_{film} decreases, the resistivity [$\rho(T)$] increases for both crystalline directions. Notably, the electrical resistivities along the $\langle 1\bar{1}0 \rangle$ and $\langle 001 \rangle$ directions exhibit distinct values. This behavior is different from bulk RuO_2 samples, where the measured resistivity is nearly identical irrespective of crystal orientations [15,16]. For $t_{film} \geqslant 3.6$ nm, the resistivity along the $\langle 1\bar{1}0 \rangle$ direction ($\rho_{\langle 1\bar{1}0 \rangle}$) surpasses that along the $\langle 001 \rangle$ direction ($\rho_{\langle 001 \rangle}$) at all temperatures. However, as the film thickness drops below 3.6 nm, this trend reverses and is quantitatively illustrated in Fig. 1(b), where we plot the resistivity ratio ($\rho_{\langle 001 \rangle}/\rho_{\langle 1\bar{1}0 \rangle}$) for the two crystal directions as a function of t_{film} at two different temperatures. Notably, the anisotropy in resistivity is independent of the temperature suggesting that its evolution with thickness is likely connected to structural changes rather than change in transport governing
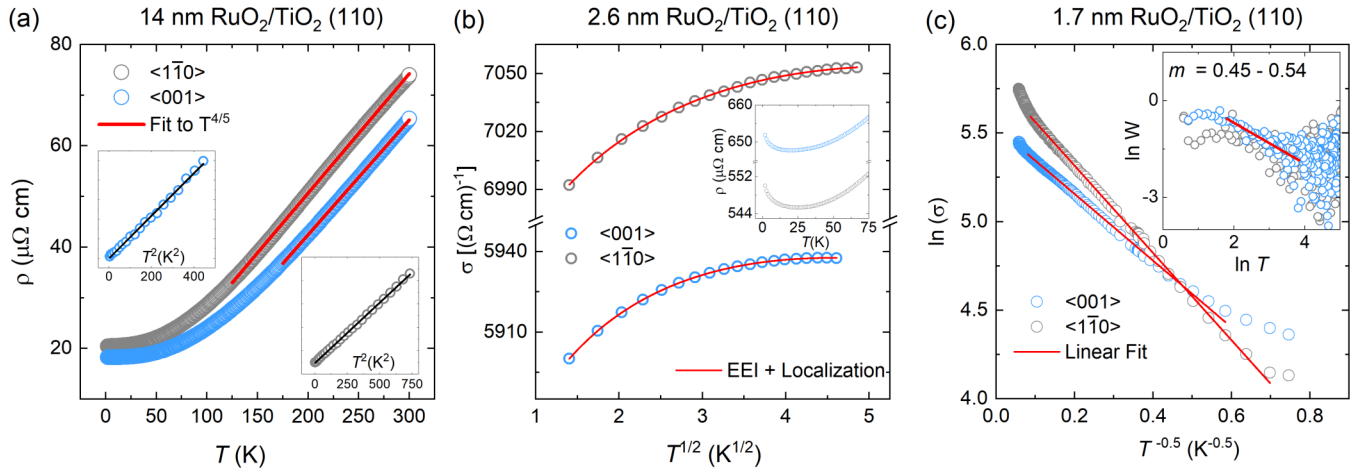
FIG. 2. (a) Resistivity vs temperature for the metallic 14 nm film. The straight line corresponds to the fits for $T^{4/5}$ behavior. The insets show resistivity vs T^2 for temperatures below 25 K. The solid black line in the inset shows the linear fit to the data. (b) Conductivity as a function of $T^{1/2}$ for 2.6 nm film. The fits are the correction to conductivity using electron-electron interaction and localization effect. The inset shows low temperature upturn in resistivity on a linear scale. (c) Logarithm of conductivity as a function of $T^{-1/2}$ for the 1.7 nm film. The inset shows the Zabrodski plot with slope $\frac{1}{2}$.

phenomena. For $t \geqslant 6$ nm, the anisotropy in resistivity tends to saturate to about 0.9, as opposed to 1 in bulk single crystal [15,16], potentially due to strain relaxation induced defects in the thin films. Interestingly, this thickness value also coincides with the onset of strain relaxation [25]. It is further noted in Ref. [25] that the strain relaxation behavior is not instantaneous with increasing film thickness but rather it is a gradual process which may be related to the monotonic decrease in anisotropy in resistivity. The dependence of resistivity on film thickness, showcasing this anisotropic behavior, implies the existence of a complex strain relaxation mechanism in rutile RuO$_2$ films grown on TiO$_2$ (110) substrates and associated electronic structure changes briefly discussed in the Introduction. Prior studies also support the thickness-driven strain relaxation in RuO$_2$/TiO$_2$(110) [19,20,25]. It is also worth noting that anisotropic strain relaxation mechanisms are known to impact orbital occupancy [27] and induce phase separation [28] in rutile VO$_2$.

We further analyzed the mechanisms governing transport behavior in these films by examining ρ vs T data presented in Fig. 1(c). We divided these films into three distinct thickness regimes: (1) thick films ($t_{film} \geqslant 3.6$ nm), where films remain metallic down to the lowest temperature (1.8 K) in our measurements. These films also possess $\rho < 150 \, \mu\Omega$ cm at 300 K. (2) Intermediate thickness ($t_{film} = 2.6$ and 2.1 nm): In this regime, films exhibited a slight upturn in the resistivity at low temperature [marked by an arrow in Fig. 1(b)], and a value exceeding 150 $\mu\Omega$ cm at 300 K. The threshold resistivity of the $\sim 150 \, \mu\Omega$ cm regime falls well under the Mooij criterion [29], suggesting that the upturn in the resistivity is due to carrier localization. (3) Ultrathin films ($t_{film} \leqslant 1.7$ nm) where the resistivity increases with decreasing T for all temperatures $\leqslant 300$ K. For $t_{film} = 1.7$ nm, resistivity approaches nearly 5000 $\mu\Omega$ cm at room temperature (equivalent to the quantum resistance, $h/e^2 \sim 26 \, k\Omega/\square$), suggesting a crossover from weak to strong localization. The insulating behavior appears at considerably lower thickness compared to the RuO$_2$ (100)

films (8 nm) in Ref. [30], likely due to lower disorder in our MBE-grown films.

Figure 2(a) shows ρ vs T data for 14 nm RuO$_2$/TiO$_2$ (110) exhibiting metallic behavior down to 1.8 K along both crystalline directions $\langle 1\bar{1}0 \rangle$ and $\langle 001 \rangle$. The residual resistivity (ρ_0) value is between 18 and 20 $\mu\Omega$ cm at 1.8 K, comparable to or lower than the previously reported values [19,20]. Insets show ρ vs T [2] data with a linear fit (solid black line) for 1.8 K $< T < 25$ K, suggesting the resistivity takes the form $\rho = \rho_0 + AT^n$, where the value of n gives information about the scattering mechanisms and A is the resistance prefactor for the corresponding scattering type [31]. The value of $n = 2$ for 1.8 K $\leqslant T \leqslant 25$ K suggests a Fermi liquid behavior with electron-electron scattering as the dominating mechanism with $A = 2 \times 10^{-4}$–$5 \times 10^{-4} \, \mu\Omega$ cm K^{-2} along both crystallographic directions. For moderate temperatures, 25 K $< T \leqslant 150$ K, $\rho(T)$ deviates from the Fermi liquid behavior, with $n < 2$. For $T \geqslant 150$ K, the value of n is $\frac{4}{5}$ [see solid red line in Fig. 2(a)], with $\delta\rho/\delta T \sim 1 \, \mu\Omega$ cm K^{-1}.

The value of $n < 1$ is typically not expected below the Debye temperature and usually is found in systems where the resistivity approaches saturation or the Mott-Ioffe-Regel (MIR) limit ($\sim 150 \, \mu\Omega$ cm) [32]. In our case, since these films are well below the MIR limit, we hypothesize that $n = \frac{4}{5}$ is due to modified phonon modes (soft phonon modes have been theoretically predicted in Ref. [20]) and the Debye temperature in our films is lower than 300 K. In fact, the reported [33] Debye temperature for a 20 nm film is 315 K, very different from the bulk value of 640 K [34]. Additionally, the Debye temperature has also been shown to decrease with decreasing film thickness of RuO$_2$ (100) [30]. Nonetheless, to avoid any misinterpretation, we note that these results do not provide direct evidence of soft phonon modes, but rather suggest an interesting possibility that future work should be directed to investigate potential connections between sublinear slope and the soft phonon modes.
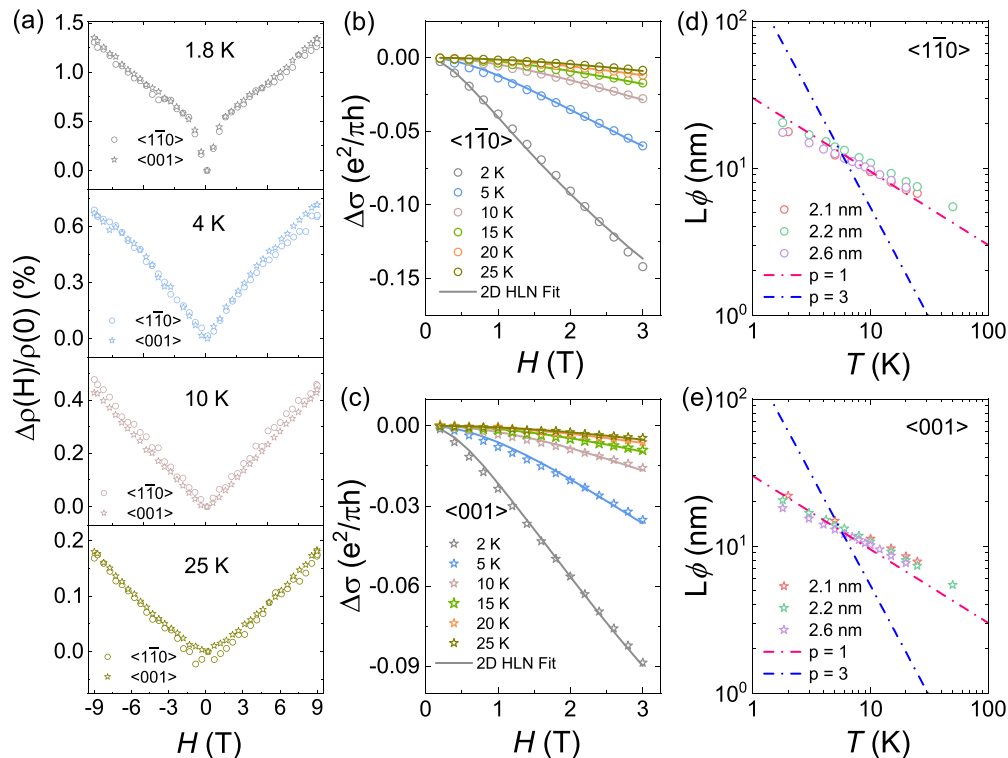
FIG. 3. (a) Magnetoresistance in a perpendicular magnetic field for the 2.1 nm thick film at various temperatures. Magnetoconductance as a function of magnetic field for (b) $\langle 1\bar{1}0 \rangle$ and (c) $\langle 001 \rangle$ crystalline directions including their fits to the 2D HLN model. Temperature dependence of inelastic scattering length for (d) $\langle 1\bar{1}0 \rangle$ and (e) $\langle 001 \rangle$ for three different samples showing weak antilocalization. The pink and blue dashed lines are theoretical curves for $p = 1$ and $p = 3$, respectively.

We next examine the transport properties of the films in the intermediate thickness regime near the metal-to-insulator transition. For the intermediate thickness regime, we first check the transport dimensionality by comparing the carrier mean free path to the film thickness. The carrier mean free path is given by $l = h/\rho n e^2 \lambda_F$, where $\lambda_F = 2(\pi/3n)^{1/3}$. Here n is carrier density, λ_F is the Fermi wavelength, e is the electron charge, and h is Planck's constant. For $n \sim 10^{23}$ cm^{-3}, which are typical values in our films, λ_F is ~ 5 Å. The calculated values of $l \sim 5$ Å are much smaller than the individual film thicknesses studied in this work, suggesting the carrier transport in these films is three dimensional (3D). The low temperature dependence of conductivity in 3D disordered systems is given by [31]

$$\sigma = \sigma_0 + A T^{1/2} + B T^{p/2}. \qquad (1)$$

The second term arises due to the electron-electron interactions (EEIs) and the third term is the correction to zero temperature conductivity due to localization effects. A and B are prefactors. The temperature dependence of the localization effect is determined from the temperature dependence of the scattering rate $\tau_\phi^{-1} = T^p$ of the dominant dephasing mechanism [35]. Figure 2(b) shows conductivity as a function of $T^{1/2}$ for the 2.6 nm film. Excellent agreement is shown between the data and Eq. (1) (red solid line), suggesting the presence of both EEI and localization effects in our thin films. The value of p is 3 for electron-phonon scattering, while it is 2 and $\frac{3}{2}$ for inelastic electron-electron collisions in the clean and dirty limit, respectively [31]. The extracted p values lie

between 1.5 and 2, suggesting the dephasing mechanism at low temperatures is mediated by inelastic electron-electron collisions but not electron-phonon scattering.

While the scattering rate due to EEI is sensitive to temperature, the localization effects are mainly limited by magnetic fields as they are averaged quantum effects. The application of a small magnetic field can destroy the time reversal symmetry which then breaks the phase coherence between the self-intersecting scattering paths of electron partial waves scattered by impurities. Therefore, temperature-dependent magnetoresistance (MR) measurements were performed to determine the dominant contribution to the low temperature resistivity upturn behavior in our films. Prior to discussing the data as presented in Fig. 3, we discuss the transport property of the film in the ultrathin regime ($t_{\text{film}} = 1.7$ nm), where strong localization exists. Here, we expect the low temperature conduction to occur via carrier hopping between the localized states, governed by variable range hopping (VRH) type conduction. The temperature dependence of hopping conduction is given by Eq. (2) [36],

$$\sigma = C \exp[-(T_0/T)^m], \qquad (2)$$

where T_0 is related to the density of localized states at the Fermi level and $m = 1/(d + 1)$ for a noninteracting d-dimensional system. Attempts to fit the logarithm of sheet conductance of the 1.7 nm film as a function of $1/T^m$ for a 3D system ($m = \frac{1}{4}$) and for a dimensional crossover from a 3D metallic state to a two-dimensional (2D) insulating state ($m = \frac{1}{3}$) were not successful. Finally, by considering the role

of Coulomb interactions [37], where $m = \frac{1}{2}$, excellent agreement with linear dependence is achieved in the temperature range 250–4.2 K, as shown in Fig. 2(c). The slope of the Zabrodski plot [36], a log-log plot of the reduced activation energy, $W = \frac{d \ln \rho(T)}{d \ln T}$ vs T, in the inset of Fig. 2(c) is $\sim \frac{1}{2}$. This observation supports our hypothesis of the role of Coulomb interactions on the conduction in the insulating regime and that the carrier transport is governed by Efros-Shklovskii variable range hopping (ES-VRH)[37].

We now turn to the discussion of temperature-dependent MR measurements in Fig. 3 to determine the dominant contribution to the low temperature resistivity upturn for the intermediate thickness range. Figure 3(a) shows $\Delta\rho/\rho$ as a function of applied magnetic field (H) in the temperature range where an upturn in resistivity is observed for the 2.1 nm thickness. At high fields ($H \geqslant \pm 3$ T), we observe positive MR which is quasilinear at all temperatures, qualitatively different from the H^2 relationship observed by Liu *et al.* [33]. In contrast, with decreasing temperature, the low-field MR (-3 T $\leqslant H \leqslant +3$ T) is qualitatively different showing a narrow cusplike positive MR at 1.8 K, in agreement with Liu *et al.* [33]. This positive (negative) interference correction to the low-field MR is known as the weak antilocalization (WAL) [weak localization (WL)] effect and it can be destroyed by the application of a magnetic field $H \geqslant H_\phi = h/(8\pi e l_\phi^2)$, where l_ϕ is the phase coherence length.

The correction to the conductance is given by 2D WAL theory [38] and can be quantified using the Hikami-Larkin-Nagaoka (HLN) model:

$$\Delta\sigma(H) \cong \alpha(e^2/\pi h)f(H_\phi/H), \qquad (3)$$

where $f(z) \equiv \ln z - \psi(\frac{1}{2} + z)$, with ψ being the digamma function and the value of $\alpha = \frac{1}{2}$ and 1 for one and two independent conduction channels, respectively [39]. In the absence of spin-orbit coupling and assuming a single conducting channel, Eq. (3) has only one fitting parameter l_ϕ, which can be determined by fitting the MR data. l_ϕ decreases with increasing temperature and is proportional to $T^{-p/2}$, where the value of exponent p depends on the dephasing mechanisms. For EEI, p takes values of 0.66, 1, and 1.5 for one, two, and three dimensions, respectively, while it is 2–4 for electron-phonon interactions [40]. Figures 3(b) and 3(c) show the magnetoconductance data along the $\langle 1\bar{1}0 \rangle$ and $\langle 001 \rangle$ crystallographic directions for films of thickness ~ 2 nm. Excellent fits to Eq. (3) are achieved, allowing us to determine l_ϕ as a function of temperature. The extracted l_ϕ are greater than the film thicknesses for all temperatures, which suggest a 2D nature of WAL. l_ϕ decreases with T and from the log-log plot of l_ϕ vs T [Figs. 3(d) and 3(e)], we determine the value of p to be ~ 0.76, suggesting a quasi-1D EEI as the dephasing mechanism.

IV. CONCLUSION

In conclusion, we have observed anisotropic electron transport in ultrathin films of RuO$_2$. With decreasing thicknesses, resistivity anisotropy increases accompanied by a crossover at $t_{film} = 3.6$ nm where the resistivity along $\langle 001 \rangle$ exceeds that along the $\langle 1\bar{1}0 \rangle$ direction. We attribute this resistivity anisotropy to anisotropic strain relaxation and associated electronic structure changes at the Fermi level. A metal-to-insulator transition is also observed with decreasing film thickness. The metallic films show a sublinear temperature dependence for 150 K $< T < 300$ K, suggesting a possible influence of strain modified phonon spectrum. Insulating behavior is explained by the presence of a Coulomb gap giving rise to ES-VRH type conduction. The electrical transport studies from the intermediate thickness regime suggest the transition to insulating behavior is facilitated by both EEI and weak antilocalization. A detailed investigation of the magnetotransport properties suggests the dominant dephasing mechanism is through electron-electron interaction. Our study thus provides insights into the understanding of electronic transport in ultrathin films of RuO$_2$ which will further add to the ongoing study on the origins of superconductivity, magnetic order, spin currents, and their manipulation using epitaxial growth techniques.

All data needed to evaluate the conclusions of the paper are present in the paper and/or the Supplemental Material [26].

[1] H. Over, Surface chemistry of ruthenium dioxide in heterogeneous catalysis and electrocatalysis: From fundamental to applied research, Chem. Rev. **112**, 3356 (2012).

[2] H. D. Kim, H. J. Noh, K. H. Kim, and S. J. Oh, Core-level x-ray photoemission satellites in ruthenates: A new mechanism revealing the Mott transition, Phys. Rev. Lett. **93**, 126404 (2004).

[3] W. D. Ryden and A. W. Lawson, Magnetic susceptibility of IrO_2 and RuO_2, J. Chem. Phys. **52**, 6058 (1970).

[4] T. Berlijn, P. C. Snijders, O. Delaire, H. D. Zhou, T. A. Maier, H. B. Cao, S. X. Chi, M. Matsuda, Y. Wang, M. R. Koehler, P. R. C. Kent, and H. H. Weitering, Itinerant antiferromagnetism in RuO_2, Phys. Rev. Lett. **118**, 077201 (2017).

[5] Z. H. Zhu, J. Strempfer, R. R. Rao, C. A. Occhialini, J. Pelliciari, Y. Choi, T. Kawaguchi, H. You, J. F. Mitchell, Y. Shao-Horn, and R. Comin, Anomalous antiferromagnetism in metallic RuO_2 determined by resonant x-ray scattering, Phys. Rev. Lett. **122**, 017202 (2019).

[6] O. Fedchenko, J. Minár, A. Akashdeep, S. W. D'Souza, D. Vasilyev, O. Tkach, L. Odenbreit, Q. Nguyen, D. Kutnyakhov, N. Wind, L. Wenthaus, M. Scholz, K. Rossnagel, M. Hoesch, M. Aeschlimann, B. Stadtmüller, M. Kläui, G. Schönhense, T. Jungwirth, A. B. Hellenes *et al.*, Observation of time-reversal symmetry breaking in the band structure of altermagnetic RuO_2, Sci. Adv. **10**, eadj4883 (2019).

[7] Z. Feng, X. Zhou, L. Šmejkal, L. Wu, Z. Zhu, H. Guo, R. González-Hernández, X. Wang, H. Yan, P. Qin, X. Zhang, H. Wu, H. Chen, Z. Meng, L. Liu, Z. Xia, J. Sinova, T. Jungwirth, and Z. Liu, An anomalous Hall effect in altermagnetic ruthenium dioxide, Nat. Electron. **5**, 735 (2022).

[8] S. Gyo Jeong, I. H. Choi, S. Nair, L. Buiarelli, B. Pourbahari, J. Y. Oh, N. Bassim, A. Seo, W. S. Choi, R. M. Fernandes, T. Birol, L. Zhao, J. S. Lee, and B. Jalan, Altermagnetic polar metallic phase in ultra-thin epitaxially-strained RuO_2 films, arXiv:2405.05838.

[9] H. Bai, L. Han, X. Y. Feng, Y. J. Zhou, R. X. Su, Q. Wang, L. Y. Liao, W. X. Zhu, X. Z. Chen, F. Pan, X. L. Fan, and C. Song, Observation of spin splitting torque in a collinear antiferromagnet RuO_2, Phys. Rev. Lett. **128**, 197202 (2022).

[10] A. Bose, N. J. Schreiber, R. Jain, D. F. Shao, H. P. Nair, J. X. Sun, X. S. Zhang, D. A. Muller, E. Y. Tsymbal, D. G. Schlom, and D. C. Ralph, Tilted spin current generated by the collinear antiferromagnet ruthenium dioxide, Nat. Electron. **5**, 267 (2022).

[11] R. Gonzalez-Hernandez, L. Smejkal, K. Vyborny, Y. Yahagi, J. Sinova, T. Jungwirth, and J. Zelezny, Efficient electrical spin splitter based on nonrelativistic collinear antiferromagnetism, Phys. Rev. Lett. **126**, 127701 (2021).

[12] D. F. Shao, S. H. Zhang, M. Li, C. B. Eom, and E. Y. Tsymbal, Spin-neutral currents for spintronics, Nat. Commun. **12**, 7061 (2021).

[13] K. M. Glassford and J. R. Chelikowsky, Electron transport properties in RuO_2 rutile, Phys. Rev. B **49**, 7107 (1994).

[14] J. J. Lin, S. M. Huang, Y. H. Lin, T. C. Lee, H. Liu, X. X. Zhang, R. S. Chen, and Y. S. Huang, Low temperature electrical transport properties of RuO_2 and IrO_2 single crystals, J. Phys.: Condens. Matter **16**, 8035 (2004).

[15] W. D. Ryden and A. W. Lawson, Electrical transport properties of IrO_2 and RuO_2, Phys. Rev. B **1**, 1494 (1970).

[16] W. D. Ryden, A. W. Lawson, and C. C. Sartain, Temperature dependence of resistivity of RuO_2 and IrO_2, Phys. Lett. A **26**, 209 (1968).

[17] Y. Sun, Y. Zhang, C.-X. Liu, C. Felser, and B. H. Yan, Dirac nodal lines and induced spin Hall effect in metallic rutile oxides, Phys. Rev. B **95**, 235104 (2017).

[18] L. Smejkal, R. Gonzalez-Hernandez, T. Jungwirth, and J. Sinova, Crystal time-reversal symmetry breaking and sponta-

neous Hall effect in collinear antiferromagnets, Sci. Adv. **6**, eaaz8809 (2020).

[19] J. P. Ruf, H. Paik, N. J. Schreiber, H. P. Nair, L. Miao, J. K. Kawasaki, J. N. Nelson, B. D. Faeth, Y. Lee, B. H. Goodge, B. Pamuk, C. J. Fennie, L. F. Kourkoutis, D. G. Schlom, and K. M. Shen, Strain-stabilized superconductivity, Nat. Commun. **12**, 59 (2021).

[20] M. Uchida, T. Nomoto, M. Musashi, R. Arita, and M. Kawasaki, Superconductivity in uniquely strained RuO_2 films, Phys. Rev. Lett. **125**, 147001 (2020).

[21] C. A. Occhialini, L. G. P. Martins, S. Fan, V. Bisogni, T. Yasunami, M. Musashi, M. Kawasaki, M. Uchida, R. Comin, and J. Pelliciari, Strain-modulated anisotropic electronic structure in superconducting RuO_2 films, Phys. Rev. Mater. **6**, 084802 (2022).

[22] B. Z. Gregory, J. Strempfer, D. Weinstock, J. P. Ruf, Y. Sun, H. Nair, N. J. Schreiber, D. G. Schlom, K. M. Shen, and A. Singer, Strain-induced orbital-energy shift in antiferromagnetic RuO_2 revealed by resonant elastic x-ray scattering, Phys. Rev. B **106**, 195135 (2022).

[23] W. Nunn, A. K. Manjeshwar, J. Yue, A. Rajapitamahuni, T. K. Truttmann, and B. Jalan, Novel synthesis approach for "stubborn" metals and metal oxides, Proc. Natl. Acad. Sci. USA **118**, e2105713118 (2021).

[24] S. Nair, Z. Yang, D. Lee, S. Guo, J. T. Sadowski, S. Johnson, A. Saboor, R. B. Comes, W. Jin, K. A. Mkhoyan, A. Janotti, and B. Jalan, Engineering metal oxidation using epitaxial strain, Nat. Nanotechnol. **18**, 1005 (2023).

[25] W. Nunn, S. Nair, H. Yun, A. K. Manjeshwar, A. Rajapitamahuni, D. Lee, K. A Mkhoyan, and B. Jalan, Solid source metal-organic molecular beam epitaxy of epitaxial RuO_2, APL Mater. **9**, 091112 (2021).

[26] See Supplemental Material at http://link.aps.org/supplemental/10.1103/PhysRevMaterials.8.075002 for structure and surface characterization of ultrathin RuO_2 films.

[27] N. B. Aetukuri, A. X. Gray, M. Drouard, M. Cossale, L. Gao, A. H. Reid, R. Kukreja, H. Ohldag, C. A. Jenkins, E. Arenholz, K. P. Roche, H. A. Durr, M. G Samant, and S. S. P. Parkin, Control of the metal-insulator transition in vanadium dioxide by modifying orbital occupancy, Nat. Phys. **9**, 661 (2013).

[28] M. K. Liu, M. Wagner, E. Abreu, S. Kittiwatanakul, A. McLeod, Z. Fei, M. Goldflam, S. Dai, M. M. Fogler, J. Lu, S. A. Wolf, R. D Averitt, and D. N. Basov, Anisotropic electronic state via spontaneous phase separation in strained vanadium dioxide films, Phys. Rev. Lett. **111**, 096602 (2013).

[29] J. H. Mooij, Electrical-conduction in concentrated disordered transition-metal alloys, Phys. Status Solidi A **17**, 521 (1973).

[30] D. Kutsuzawa, D. Oka, and T. Fukumura, Thickness effects on crystal growth and metal–insulator transition in Rutile-Type RuO_2 (100) thin films, Phys. Status Solidi B **257**, 2000188 (2020).

[31] P. A. Lee and T. V. Ramakrishnan, Disordered electronic systems, Rev. Mod. Phys. **57**, 287 (1985).

[32] N. E. Hussey II, K. Takenaka, and H. Takagi, Universality of the Mott–Ioffe–Regel limit in metals, Philos. Mag. **84**, 2847 (2004).

[33] J. Liu, L. Gao, Y. T. Zou, T. Lin, M. T. Zhu, X. Y. Lyu, C. Lu, Y. Q. Wang, A. L. Ji, Q. H. Zhang, Z. G. Cheng, L. Gu, Z. X. Cao, and N. P. Lu, Emergent weak antilocalization and wide-temperature-range electronic phase diagram in epitaxial RuO_2 thin film, J. Phys.: Condens. Matter **35**, 405603 (2023).

[34] B. C. Passenheim and D. C. McCollum, Heat capacity of RuO_2 and IrO_2 between 0.54° and 10° K, J. Chem. Phys. **51**, 320 (1969).

[35] J. J. Lin and J. P. Bird, Recent experimental studies of electron dephasing in metal and semiconductor mesoscopic structures, J. Phys.: Condens. Matter **14**, R501 (2002).

[36] N. F. Mott, Conduction in non-crystalline materials, Philos. Mag. **19**, 835 (1969).

[37] A. L. Efros and B. I. Shklovskii, Coulomb gap and low-temperature conductivity of disordered systems, J. Phys. C: Solid State. **8**, L49 (1975).

[38] S. Hikami, A. I. Larkin, and Y. Nagaoka, Spin-orbit interaction and magnetoresistance in the 2 dimensional random system, Prog. Theor. Phys. **63**, 707 (1980).

[39] I. Garate and L. Glazman, Weak localization and antilocalization in topological insulator thin films with coherent bulk-surface coupling, Phys. Rev. B **86**, 035422 (2012); **86**, 039909(E) (2012).

[40] B. L. Altshuler, A. G. Aronov, and D. E. Khmelnitsky, Effects of electron-electron collisions with small energy transfers on quantum localization, J. Phys. C: Solid State **15**, 7367 (1982).